Magnetic Resonance Imaging Study of Current and Ion Delivery into the Eye during Transscleral and Transcorneal Iontophoresis

S. Kevin Li,[1] *Eun-Kee Jeong,*[2] *and Matthew S. Hastings*[1,3]

Purpose. The objectives were to determine by nuclear magnetic resonance imaging (MRI) the target sites of ion delivery in the eye during iontophoresis, compare transscleral and transcorneal ocular iontophoresis, and monitor the distribution of a probe ion in the anterior chamber and vitreous after iontophoretic delivery.

Methods. Thirty-minute 2-mA anodal constant current transscleral and transcorneal iontophoresis (current density, 10 mA/cm^2) was performed on three New Zealand White rabbits in vivo. Intravitreal injection and passive delivery were the controls. Transscleral and transcorneal iontophoresis experiments were conducted with the electrode device placed in the superior cul-de-sac away from the limbus and on the cornea adjacent to the limbus, respectively. During iontophoresis, the current delivered into the eye was monitored using a probe ion (Mn^{2+}) with MRI. The distributions of the ion in the aqueous and vitreous humor after iontophoresis, passive delivery, and intravitreal injection were also determined by MRI.

Results. With the short application time, passive diffusion did not deliver a significant amount of the ion into the eye. Whereas transscleral iontophoresis delivered the ion into the vitreous, transcorneal iontophoresis delivered the ion into the anterior chamber. The current pathways during iontophoresis were mainly from the electrode into the eye, perpendicular to the electrode–eye interface beneath the electrode. Electric current along the surface of the globe was relatively minimal. With the present transscleral iontophoresis protocol, the ion penetrated the sclera and traveled as far as 1.5 mm from the electrode–conjunctiva interface into the vitreous. For transcorneal iontophoresis, the ion penetrated the cornea and filled the entire anterior chamber.

Conclusions. MRI can be a useful technique in the study of the penetration of probe compounds in the eye during and after iontophoresis, such as in iontophoresis protocol and device testing. Ocular pharmacokinetic studies using MRI are noninvasive and provide real-time data without perturbation and compound redistribution that can occur during dissection and assay in traditional pharmacokinetic studies. With MRI, it was shown that transscleral iontophoresis, transcorneal iontophoresis, and intravitreal injection deliver ions to different parts of the eye. (*Invest Ophthalmol Vis Sci.* 2004;45:1224–1231) DOI:10.1167/iovs.03-0821

Because drugs do not usually penetrate the posterior segment of the eye after topical administration of eye drops, systemic drug administration and direct injections (intravitreal and periocular) are common methods for the treatments of posterior eye diseases. However, both methods have their drawbacks. Systemic administration is usually not preferred because of the systemic toxicity involved. Repeated treatments with injections may lead to complications and patient discomfort.[1] Iontophoresis is a method used to deliver a compound across a membrane by the assistance of an electric field. This method has been extensively studied in other routes of drug administration such as in transdermal iontophoresis.[2–6] Ocular iontophoresis was first studied for the treatment of ocular inflammation with steroids several decades ago.[7] Recently, this technique has been applied to different drugs in the treatments of different eye diseases.[8–12] In ocular iontophoresis, a donor electrode containing the drug to be delivered into the eye is placed on the eye, and the other electrode referred to as the return electrode is placed on another body surface, forming an electrical circuit through the body. Because of the separated components of the eye, the current pathways driven across the eye between the donor and the return electrodes can vary, depending on many different factors. In addition, the thickness of the sclera hemisphere is not uniform. The current pathways in the eye during iontophoresis are therefore not well defined. Without the knowledge of the sites in the eye to which ions are delivered during ocular iontophoresis, improvements to the technology for effective drug delivery to different parts in the eye cannot be easily achieved.

Manganese (Mn) is a common contrast agent used in MRI. For example, it has been used in the imaging of the liver[13] and in neuroaxonal tracing of the optic nerve.[14] Manganese-enhanced magnetic resonance imaging (ME-MRI) works under the principle that Mn^{2+} ion enhances the relaxivity of the water protons, reducing the proton spin-lattice relaxation times (T_1). As a result, T_1-weighted MR images show enhanced signal intensities at the locations of the Mn^{2+} ions. The higher the concentration of Mn^{2+} ion in the vicinity, the more the signal is enhanced. ME-MRI is a noninvasive method of studying ocular iontophoresis. The approach not only reduces the number of animals required in pharmacokinetic studies, but it also allows the determination of the concentration profiles in the eye (e.g., in the vitreous) in real time.

In the present study, the target sites of ion delivery and the electric current pathways during transscleral and transcorneal iontophoresis were to be determined and compared using MRI in a rabbit model in vivo. Intravitreal injection and passive delivery were the controls. The distributions of the probe ion after iontophoresis, intravitreal injection, and passive delivery were also to be monitored with MRI. These results should improve our understanding of ocular iontophoresis and help in the optimization of ocular iontophoresis for site-specific drug delivery into the eye.

From the [1]Department of Pharmaceutics and Pharmaceutical Chemistry and the [2]Utah Center for Advanced Imaging Research (Radiology), University of Utah, Salt Lake City, Utah; and [3]Aciont Inc., Salt Lake City, Utah.

Supported in part by National Institutes of Health Grant GM063559.

Submitted for publication August 1, 2003; revised October 4 and December 12, 2003; accepted December 17, 2003.

Disclosure: **S.K. Li**, Aciont Inc. (F, C); **E.-K. Jeong**, None; **M.S. Hastings**, Aciont Inc. (F, E)

The publication costs of this article were defrayed in part by page charge payment. This article must therefore be marked "*advertisement*" in accordance with 18 U.S.C. §1734 solely to indicate this fact.

Corresponding author: S. Kevin Li, Department of Pharmaceutics and Pharmaceutical Chemistry, University of Utah, Salt Lake City, UT 84112; kevin.li@m.cc.utah.edu.

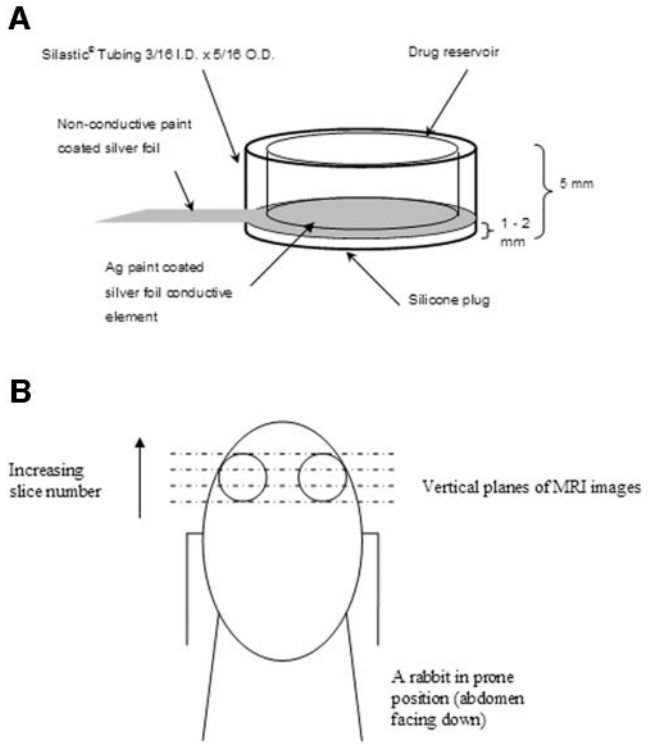

FIGURE 1. (**A**) Donor electrode device configuration. (**B**) MR imaging planes and orientation (diagram not to scale).

MATERIALS AND METHODS

Materials and Animals

$MnCl_2$ tetrahydrate was purchased from Spectrum Chemical (Gardena, CA). Agarose (Type IX) was purchased from Sigma-Aldrich (St. Louis, MO); sodium chloride USP 0.9% (pH between 5 and 7) from Baxter Healthcare (Deerfield, IL); flexible tubing (Silastic, Tygon; 3/16 in. inner diameter × 5/16 in. outer diameter) from VWR Scientific (San Francisco, CA); silver foil (1.5 in. × 0.004 in.) from EM Science (Gibbstown, NJ); and liquid silver paint was from Ladd Research Industries (Williston, VT). Three New Zealand White rabbits of 3 to 4 kg were purchased from Western Oregon Rabbit Co. (Philomath, OR) and were used as the animal model in the in vivo experiments under the approval of the Institutional Animal Care and Use Committee at the University of Utah and in compliance with the ARVO Statement for the Use of Animals in Ophthalmic and Vision Research. Enucleated rabbit eyes in the MRI calibration experiments were obtained from rabbits after they were euthanatized in other non-ocular studies at the University of Utah Animal Resource Center.

Iontophoresis Electrode Device

Flexible tubing (3/16 in. inner diameter × 5/16 in. outer diameter × 1/4 in. length; Silastic; VWR Scientific) was the outer shell of the electrode device (Fig. 1A). One end of the tubing was sealed by silicone elastomers (NuSil Technology, Carpinteria, CA), and a piece of silver foil was inserted at the back of the shell adjacent to the seal as the conductive element. A layer of liquid silver paint (~0.05 cm thick) was put on the silver surface to increase the effective surface area of the Ag electrode. The electrode chamber (donor compartment) was then filled with approximately 2% agarose gel in normal saline (0.9%) with 0.4 mM $MnCl_2$. The final volume of the agarose-filled chamber was between 0.04 and 0.07 mL. The silver surface outside the electrode was covered with a nonconductive paint. The Ag/AgCl return electrode was prepared by electrochemically plating a silver sheet in saturated KCl solution.

MRI Data Acquisition

MRI experiments were performed with a clinical MRI system (1.5-T GE Signa [NV/CVi gradient] Milwaukee, WI). A temporal mandibular joint (TMJ) coil, a double-surfaced phased-array coil set 3-in in diameter, was used. Dynamic MR imaging was performed with a T_1-weighted, spin-echo imaging method. Unless otherwise specified, the imaging parameters were 400-ms repetition time (*TR*), 9-ms echo delay time (*TE*), 256 readout matrix with 160 phase-encoding, two signal averages to increase signal-to-noise ratio (SNR). The field of view (FOV) was 8 cm for a single eye or 12 cm for imaging both eyes in a single scan. Rectangular FOV with 50% reduction factor was used to reduce the imaging time, which produced the actual FOV of 8 cm along readout and 4 cm along phase-encoding directions for 8 cm FOV imaging. The slice thickness was 2 mm with no spacing (Fig. 1B), resulting in spatial resolution of $0.47 \times 0.47 \times 2.0$ mm^3. Prescanning was performed only once for the first data set before the onset of the experiment, and the imaging parameters including the prescan results, such as transmitter and receiver gains, were fixed. Imaging time for single-time data was approximately 1 minute for 4-minute temporal resolution. The MR images were analyzed on a PC computer (Scion Image software; Scion Corp., Frederick, MD).

It should be pointed out that the effects of the strong magnetic fields on the applied iontophoretic current and Mn^{2+} ion are negligible. The equivalent electric field on the ions due to the Lorentz force is insignificant compared with the electric field, *E*, provided by iontophoresis. Briefly, $F_c = (ev) \times B$, where F_c is force, *e* is charge, *B* is magnetic field, and *v* is charge velocity. When the magnetic field is perpendicular to the current (i.e., maximum effect), $F_c = evB$. The force on an ion during iontophoresis is related to the electric field, $F_c = eE$. Combining these two equations, $E = vB$. When $B = 1.5$ T and $v \approx 6 \times 10^{-6}$ m/s (ion velocity normally encountered during iontophoresis: 6×10^{-4} cm^2/s per V at 1 V/cm), $E = 9 \times 10^{-6}$ V/m, which is negligible compared with the applied electric fields in the present iontophoresis study. Furthermore, the distribution of Mn^{2+} ion in aqueous solution is homogeneous in the bore magnet, suggesting that the effects of the magnetic force on the ion are insignificant relative to Brownian motion.

MRI Calibration

The signal equation of the spin-echo imaging is

$$\frac{S_I}{S_0} = (1 - e^{-(TR-0.5TE)/T_1})\, e^{-TE/T_2} \qquad (1)$$

where S_I is the signal intensity, S_0 is the intrinsic fully recovered signal intensity, T_1 is the spin–lattice relaxation time, and T_2 is the spin–spin relaxation time. When $TR \gg TE$, the signal equation can be simplified as[15]:

$$\frac{S_I}{S_0} = (1 - e^{-TR/T_1})\, e^{-TE/T_2} \qquad (2)$$

Experiments were conducted to create a calibration curve between manganese-enhanced signal intensity and Mn^{2+} concentration. $MnCl_2$ standard solutions of 0.01 to 4 mM Mn^{2+} were prepared in saline and in deionized water. The solutions (~5 mL in capped glass vials) were imaged with spin-echo pulse sequences: *TR* was 50, 100, 200, 400, 800, 1600, and 2400 ms, with *TE* fixed at 9 ms for T_1 measurements, and *TE* was 15, 30, 45, and 60 ms, with *TR* fixed at 2400 ms for T_2 measurements. The relaxation times T_1 and T_2 of these standards were determined by curve fitting of the signal intensity of a region-of-interest (ROI) with respect to the time variables *TE* and *TR*, using equation 2. This experiment allowed us to determine the concentrations of Mn^{2+} by direct comparison and correct for T_2 effects at higher concentrations of the contrast agent.

Calibration experiments to identify possible Mn^{2+} binding in the eye were conducted with enucleated eyes and extracted vitreous humor in vitro. In the equilibration experiments with enucleated rabbit eyes, the eyes were equilibrated in 100 mL $MnCl_2$ solutions of 0.04 to 1 mM Mn^{2+} in saline for 48 hours. The eyes were then removed from the solutions and scanned. In the experiments with rabbit vitreous humor, the vitreous humor was extracted from freshly excised eyes. Known amounts of concentrated Mn^{2+} solutions were then added to the vitreous humor in vials. The T_1 of Mn^{2+} in vitreous humor and in saline was compared.

In Vivo Experiments

Transscleral and transcorneal iontophoresis experiments were conducted on three rabbits. After the rabbits were anesthetized with 1 mg/kg diazepam intraperitoneally (IP), 0.1 mg/kg glycopyrrolate intramuscularly (IM), 25 to 50 mg/kg ketamine IM, and 5 to 10 mg/kg xylazine IM, an electrode device with $MnCl_2$ was placed on the conjunctiva–sclera in the superior cul-de-sac (under the upper eyelid) away from the limbus or on the cornea adjacent to (or touching) the limbus for transscleral and transcorneal iontophoresis, respectively. The position of the electrode for transscleral iontophoresis in the superior cul-de-sac was maintained naturally by the pressure from the eyelid. The silver foil sticking out from the electrode (Fig. 1a) was then fixed by medical adhesive tape, and the electrode in the cul-de-sac was further secured by adhesive tape over and on top of the upper and lower eyelids. The upper conjunctiva was chosen because of the larger space available for the electrode device in the superior cul-de-sac than that in the inferior cul-de-sac of rabbits. For transcorneal iontophoresis, the position of the electrode on the cornea was maintained by the pressure from the eyelid and secured by medical adhesive tape. During iontophoresis, the position of the electrode was checked by comparing the relative electrode position with the anatomic structures of the eye in the MR images. Both the left and right eyes were used, but they were not used concurrently. The return electrode (approximately 4 cm^2 surface area) was placed on a piece of gauze pad (approximately 40 cm^2 surface area) wetted in saline and clamped to the ear. A 2-mA anodal constant current DC (10 mA/cm^2) was applied to the eye for 30 minutes with a constant-current iontophoretic device (Phoresor II Auto, model PM850; Iomed, Inc., Salt Lake City, UT). The delivery and distribution of Mn^{2+} ion in the eye were monitored by MRI. At the end of the iontophoresis experiment, the pH of the electrode was checked and was found to be between pH 5 and 7. Between each experiment, the animals were allowed an approximately 1-month washout period.

A control experiment was also conducted to examine possible MR image artifacts due to the applied electric current during iontophoresis (2 mA for 30 minutes) without the presence of Mn^{2+} ion. Another control experiment involved passive delivery, using the electrode device with $MnCl_2$ as the donor but without application of electric current. The electrode device was placed on the limbus, covering parts of both the cornea and sclera. The same rabbits in the iontophoresis experiments were involved in these control experiments.

Intravitreal injections (0.1 mL) of 0.4 mM and 1.0 mM $MnCl_2$ in saline were performed with the rabbits under anesthesia. A 30-gauge 0.5-in. needle was used in this procedure. The needle was inserted at the center of the sclera surface under the upper eyelid through the sclera (conjunctiva, sclera, choroid, and retina) into the vitreous. The distribution of the ion after the injections was monitored by MRI.

Theories and Equations for Iontophoresis and Diffusion

For iontophoretic transport within and from an ocular electrode device, the conventional Nernst-Planck equation can be used. The flux, J, of an ion across a planar surface during iontophoresis is expressed as[16]

$$J = \varepsilon\left(- D\frac{dC}{dx} - uC\frac{d\psi}{dx} \pm v_f C\right) \quad (3)$$

where C, x, D, and u are the concentration, position, diffusion coefficient, and electromobility of the probe permeant, respectively; ε is the combined porosity and tortuosity factor; ψ is the electrical potential at position x; and v_f is the average velocity of the convective solvent flow resulting from pressure and electroosmosis. The flux of an ion is also related to the electric current carried by the ion as

$$J = \frac{I}{zFA} \quad (4)$$

where I is the electric current, z is the charge, F is the Faraday constant, and A is the surface area available for transport. With a constant electric field and for dominant electrophoresis transport over passive diffusion and convection, equations 3 and 4 can be combined and simplified as

$$\frac{I}{zFA} = \varepsilon uC\frac{\Delta\psi}{\Delta x} \quad (5)$$

where $\Delta\psi/\Delta x$ is the electric field applied and u ($\Delta\psi/\Delta x$) is the migration velocity. The distance of ion migration, h, can be expressed as

$$h = u\frac{\Delta\psi}{\Delta x}t \quad (6)$$

where t is time of iontophoresis application.

In the analysis of the intravitreal injection data, a simple model of passive diffusion from a spherical source can be used. The concentration at radial position r at time t, C_r, from the center of an initially uniformly distributed spherical source of concentration, C_0, and radius a is calculated by[17]

$$C_r = \frac{1}{2}C_0\left(erf\frac{a-r}{2\sqrt{Dt}} + erf\frac{a+r}{2\sqrt{Dt}}\right) - \frac{C_0}{r}\sqrt{\frac{Dt}{\pi}}\left(e^{[-(a-r)^2]/4Dt} - e^{[-(a+r)^2]/4Dt}\right) \quad (7)$$

With equation 7, the diffusion coefficient of the ion in the vitreous after intravitreal injections can be estimated under the assumptions that the bolus injection initially creates a 0.1-mL sphere of equally distributed ions in the vitreous, and there is no significant Mn^{2+} binding to proteins in the vitreous. The assumption of insignificant Mn^{2+}-protein binding is consistent with the essentially same diffusion coefficients and T_1 values of Mn^{2+} in saline and in vitreous humor discussed later in the article.

Results

MRI Calibration

Figure 2A shows the relationships of the relaxation rates $1/T_1$ and $1/T_2$ versus $MnCl_2$ concentration in saline and in deionized water. Linear relationships between the relaxation rates and Mn^{2+} concentration with positive y-intercepts are observed at the low Mn^{2+} concentration in the present study. The y-intercept of the $1/T_1$ versus concentration plot is consistent with T_1 of water in the literature (~4 seconds). There is no significant difference between the T_1 and T_2 of Mn^{2+} in deionized water and those in saline. Figure 2B presents the S_I/S_0 versus Mn^{2+} concentrations in saline and in water. As can be seen in the figure, S_I/S_0 reaches a maximum of approximately 0.5 at about 0.6 to 1.0 mM Mn^{2+} and is relatively linear with respect to Mn^{2+} concentration below 0.4 mM. The concentration of $MnCl_2$ used in the present study was therefore chosen to be 0.4 mM in saline, unless otherwise specified.

In the vitreous humor calibration experiments, the T_1 of Mn^{2+} was essentially the same in saline and in the extracted

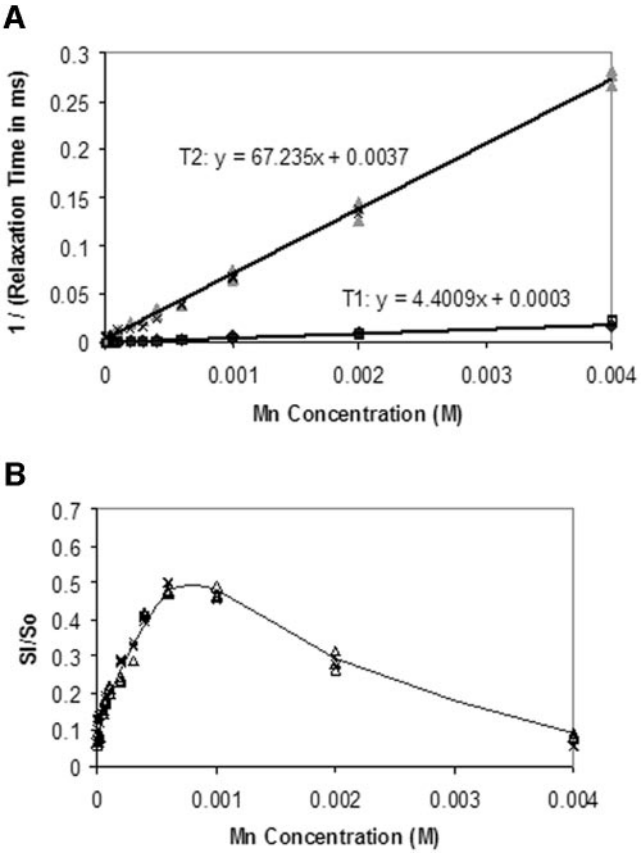

FIGURE 2. (**A**) Relationship between the inverse of relaxation time and Mn concentration. (♦) T_1 in saline, (□) T_1 in water, (△) T_2 in saline, and (×) T_2 in water. (**B**) Relationship between signal intensity ratio S_I/S_0 and Mn concentration. (△) in saline and (×) in water.

vitreous humor. When Mn^{2+} was equilibrated in the eye in vitro, the signal was essentially homogenous in the vitreous and in the anterior chamber of the eye and equal to that of the equilibrating solution. However, some structures in the eye showed significantly higher signal intensities (e.g., the cornea, sclera-retina, and ciliary body). Relaxation times in tissues are generally different from those in aqueous medium (e.g., vitreous humor). Therefore, caution should be used in interpreting the signal intensity data of the cornea and sclera-retina structures. Studies have also suggested that Mn^{2+} ions can be taken up by the retinal ganglion cells and transported along the optic axon in vivo.[14,18] Although such transport of Mn^{2+} is slow (0.28 cm/h)[14] and should not affect the distributions of Mn^{2+} in the vitreous and aqueous humor, this can complicate the interpretation of the Mn^{2+} data of the retina. Therefore, it was concluded that quantitative interpretation of the results should be limited to Mn^{2+} in the vitreous and anterior chamber in the present study.

Passive Delivery

Representative MR images during passive delivery through the electrode device are shown in Figure 3. The eyelids, anterior chamber, lens, vitreous, and other structures of the eye were visible in the MR images. Mn^{2+} in the donor compartment of the electrode device in the superior cul-de-sac appears as a high-signal-intensity rectangular shape. The outer shell of the device (background signal with an inverse U-shape) enclosing the Mn^{2+} compartment can also be seen in the superior cul-de-sac between the donor compartment and the upper eyelid.

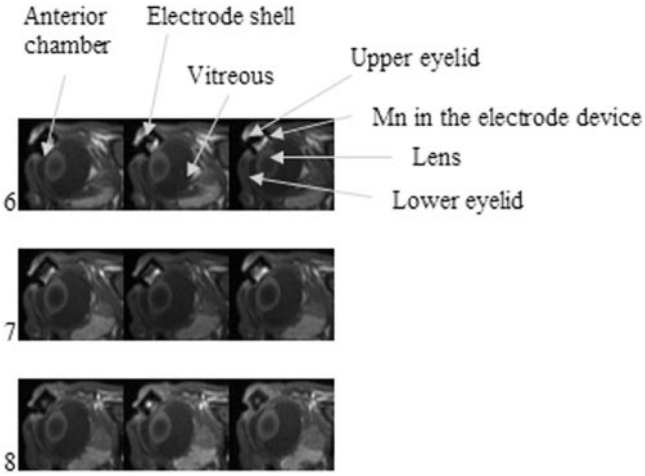

FIGURE 3. Passive transport delivery from the electrode device in vivo without the application of the current (control). *Left to right*: images taken at 8, 32, and 62 minutes after the application of the device. *Top to bottom*: images from increasing slice numbers shown at *left* (slice thickness: 2mm; see Fig. 1B). The radius of the eye is approximately 1 cm (labels apply to Figs. 3–6).

The weaker signal near the top of the Mn^{2+} compartment is due to signal interference from the Ag metal electrode. Although no external pressure was applied to the electrode device on the eye, the pressure due to the contact with the eyelid was significant and deformed the eye surface. As can be seen in Figure 3, there were no significant changes in the signal intensity of the tissues (±15%) in the eye under and around the site of the electrode application over the duration of the application. There were slightly higher signal intensities than the background control on the surface of the eye, but they were within the noise. The amount of Mn^{2+} delivered into the eye was below the detection limit of the present MRI technique (<0.02 mM).

Intravitreal Injection

The distribution of Mn^{2+} in the vitreous after intravitreal injections was determined by MRI. Figure 4 shows the MR images after 0.1-mL intravitreal injection of 1.0 mM $MnCl_2$ in saline. As expected, the lens was a barrier to the diffusion of Mn^{2+} ions. The ions did not penetrate the lens into the anterior chamber within the time frame of the MRI experiments. The data were then used to characterize the diffusion of ions in the

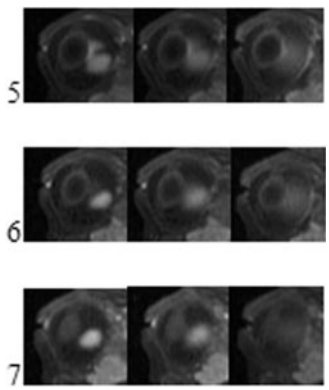

FIGURE 4. Intravitreal 0.1-mL injection of 1.0 mM $MnCl_2$ in saline in vivo. *Left to right*: images taken at 3, 13, and 53 minutes after intravitreal injection. *Top to bottom*: images from increasing slice numbers (slice thickness: 2 mm; see Fig. 1B).

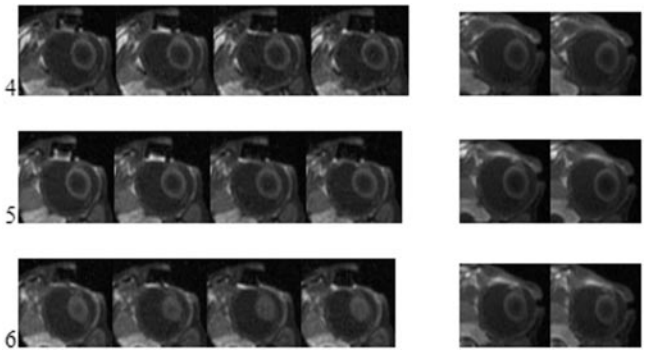

FIGURE 5. Transscleral iontophoresis in vivo. *Left to right:* images taken at 0, 9, 18, and 27 minutes during and 35 and 75 minutes after iontophoresis. *Top to bottom*: images from increasing slice numbers (slice thickness: 2 mm; see Fig. 1B).

vitreous by using equation 7. In this analysis, the average signal intensity of the center (~0.2 cm in diameter) of the Mn^{2+} spot in the vitreous (i.e., the ROI) was determined at different time points after the injection (0–35 minutes). Data points beyond 35 minutes were not used, because the free-diffusion assumption of equation 7 would not be valid when the Mn^{2+} concentration boundary reached the retinal barrier. The signal intensity was then converted to the Mn^{2+} concentration by using the S_I/S_0 versus concentration data in Figure 2B. Five times higher signal intensity at this location relative to the background (vitreous without Mn^{2+}) was observed immediately after the injection. This is consistent with the initial concentration of Mn^{2+}. Using the present method, the diffusion coefficient of Mn^{2+} in the vitreous was estimated to be 1.3×10^{-5} cm^2/s (uncertainty: $\pm 0.4 \times 10^{-5}$ cm^2/s). This value is consistent with free diffusion of Mn^{2+} in an aqueous medium and suggests that the vitreous behaves like a free aqueous diffusion medium, as stated in the literature.[19] The demonstration of free diffusion of the ion in the vitreous provides the basis of the analysis of ion distribution after iontophoresis in the present study.

Transscleral and Transcorneal Iontophoresis

Representative MR images of the eye during transscleral and transcorneal iontophoresis are shown in Figures 5 and 6, respectively. The distribution of Mn^{2+} ion up to 75 minutes after iontophoresis applications is also shown in these figures; note that the positions of the images taken during and after iontophoresis can be different. Not shown in the figures are the MR images of the eye under the same iontophoresis application

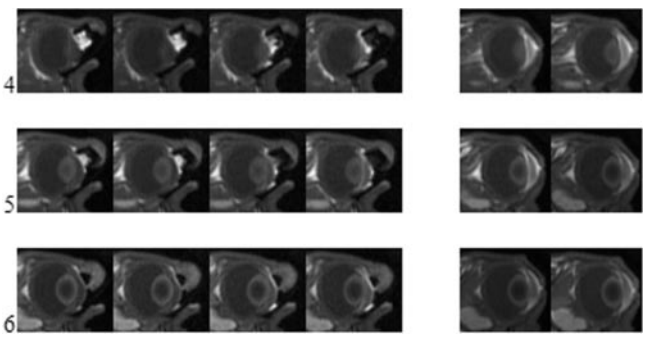

FIGURE 6. Transcorneal iontophoresis in vivo. *Left to right*: images taken at 0, 9, 18, and 27 minutes during and 32 and 65 minutes after iontophoresis. *Top to bottom*: images from increasing slice numbers (slice thickness: 2 mm; see Fig. 1B).

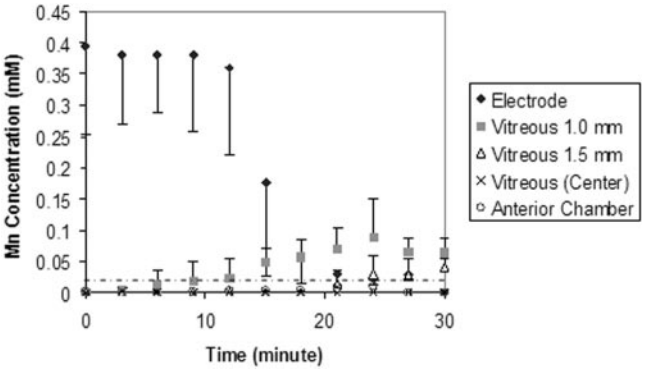

FIGURE 7. Concentration–time profiles of Mn^{2+} ions at different locations during transscleral iontophoresis. Concentration data are presented as the mean ± SD (n = 3). All data are determined from the image slice (thickness: 2 mm) sectioned across the middle of the eye and the iontophoresis electrode. (◆) In the electrode device near the device–conjunctiva interface; in the vitreous approximately (▨) 1.0 mm (ROI: ~0.5–1.5 mm) or (△) 1.5 mm (ROI: ~1.0–2.0 mm) away from the device–conjunctiva interface at the site of electrode application; (✕) at the center of the vitreous; and (○) at the center of the anterior chamber. *Dotted line*: limit of quantitative assessment in the current MRI method.

without Mn^{2+} in the donor electrode device. In this control study, no artifact was observed in the MR images of the eye during and after iontophoresis without Mn^{2+}. Figures 7 and 8 show the concentration-time profiles of Mn^{2+} at specified locations in the eye during transscleral and transcorneal iontophoresis, respectively. These concentrations were determined by the signal intensities (S_I) at the locations (i.e., the ROIs) relative to those of the background (without Mn^{2+}, S_0) at the same locations using the data in Figure 2B. The MRI data show that the concentrations of the ion in the ROIs in the vitreous and in the anterior chamber under the electrode during transscleral and transcorneal iontophoresis, respectively, reached as high as 25% of the ion concentration in the donor compartment of the electrode device. The MRI data also show that the target sites to which the ion was iontophoretically delivered into the eye (vitreous or anterior chamber) depended on the

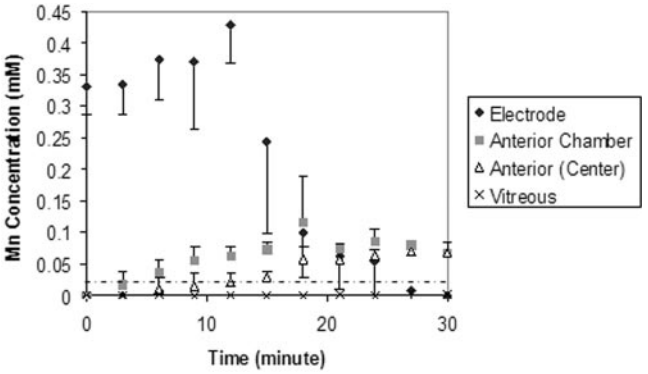

FIGURE 8. Concentration-time profiles of Mn^{2+} ion at different locations during transcorneal iontophoresis. Concentration data are presented as the mean ± SD (n = 3). All data are determined from the image slice (thickness: 2 mm) sectioned across the middle of the eye and the iontophoresis electrode. (◆) In the electrode device near the device–cornea interface; (▨) in the anterior chamber approximately 1.0 mm away from the device–cornea interface (ROI: ~0.5–1.5 mm) under the site of application; (△) at the center of the anterior chamber; and (✕) in the vitreous behind the ciliary body. *Dotted line*: limit of quantitative assessment using the current MRI method.

placement position of the electrode (i.e., transscleral versus transcorneal).

Discussion

Passive Delivery, Transscleral Iontophoresis, and Transcorneal Iontophoresis

The small amount of Mn^{2+} delivered into the eye during and after passive delivery can be due to the short application time. However, changes in the signal intensities of the eye tissues and the vitreous under the electrode were expected, because the time to establish a concentration gradient across the tissue barrier into the vitreous in passive diffusion should be shorter than 10 minutes. This amount of time is estimated using a thickness of 0.1 cm (which is approximately two times the average combined thickness of the conjunctiva and sclera) and assuming that the ion diffuses across a relatively unhindered aqueous pathway[20,21] with free diffusion coefficient of 10^{-5} cm^2/s. The inability of the ion to establish a concentration gradient over the duration of the experiment suggests that tear drainage, the conjunctiva, and/or conjunctival and choroidal vasculature clearance can be significant barriers to passive ocular drug delivery. It should also be pointed out that small changes in the concentration of Mn^{2+} in small volume may not be detectable with the spatial resolution of the present MRI study.

In contrast to passive delivery through the electrode device, significant penetration of the probe ion was observed during iontophoresis. According to the MR images in Figures 5 and 6 and the concentration data in Figures 7 and 8, both transscleral and transcorneal iontophoresis took approximately 12 to 18 minutes to unload the entire content of Mn^{2+} in the electrode device in the present study. The time to unload the entire content to the eye was independent of the sites of electrode placement. This observation is consistent with the electromobility of Mn^{2+}, the dimension of the electrode device, and the current applied. Under the electric current of 2 mA and with the electrical resistance of the donor compartment in the electrode device being approximately 0.2 kΩ, the electric field across the electrode chamber was approximately 1 V/cm. According to equation 6 and Mn^{2+} aqueous electromobility in saline of 4×10^{-4} $cm^2/s/V$, an Mn^{2+} ion traveled 0.4 cm (approximately the dimension of the electrode device) in 17 minutes at 2 mA, which is consistent with the time observed for Mn^{2+} to be completely unloaded from the electrode in the MR images.

The main distinctive feature between transscleral and transcorneal delivery was the different target sites of delivery (i.e., different current pathways). For transscleral iontophoresis, the probe ion was predominantly transported directly into the vitreous under the electrode. During the 30-minute iontophoresis transport, the ion penetrated approximately 0.1 cm into the vitreous (Fig. 7). There was no observable Mn^{2+}-enhanced signal deeper in the vitreous (above the 0.02-mM detection limit) over the duration of the experiments. This is again consistent with electrotransport theory. When the Mn^{2+} ion left the electrode chamber, the ion was driven by a weaker electric field than that within the electrode chamber, due to the distribution of the current outward in the eye from the electrode–conjunctiva interface (i.e., from the conjunctiva to the sclera and then to the vitreous). As the cross-sectional area of the current passage increased, the electric field decreased (equation 5), and the migration velocity of the ions decreased. If the electric field in the vitreous had remained the same as that in the electrode chamber, the ion front would have traveled approximately 0.6 cm into the vitreous from the device–conjunctiva interface (instead of the observed 0.1–0.2 cm) after 30 minutes of the iontophoresis application (equation 6). Some distributions of the ion along the sclera structure outward from the area beneath the electrode were also observed near the end of the iontophoresis application. The MR images also clearly showed a depot of the probe ion loaded in the conjunctiva-sclera-retina tissues under and near the site of iontophoresis (Fig. 5). The depot was beneath the surface and was not removed by tears and a saline rinse applied to the eye surface. Ion distribution by diffusion after iontophoresis occurred mainly near these tissues and was at a slower rate toward the center of the vitreous than the diffusion rate observed in the intravitreal injection experiments (Fig. 4). This is consistent with ion clearance through the retina.

In contrast to transscleral iontophoresis, the anterior chamber was the site of ion delivery in transcorneal iontophoresis. The probe ion was transported across the cornea into the anterior chamber and distributed in the aqueous humor (Figs. 6, 8). No ion was observed to be distributed into the vitreous from the anterior chamber through the posterior chamber over the duration of the experiment. It should be pointed out that ion distribution in the anterior chamber during and after transcorneal iontophoresis appeared to occur faster than that in the vitreous during transscleral iontophoresis. One explanation is the difference between the volume of the anterior chamber and that of the vitreous. It is also speculated that this may be a result of deeper penetration of the ion during iontophoresis because of the lesser divergence of the electric field, and/or ion movement due to clearance through the canal of Schlemm in the anterior chamber. Another interesting observation in the MR images during and after transcorneal iontophoresis is the pattern of Mn^{2+} distribution in the anterior chamber. A lack of probe ion in the middle of the anterior chamber was observed. This distribution pattern is not consistent with simple passive diffusion or simple current driven transport in the eye and may be related to the presence of other structures in the anterior part of the eye (e.g., iris) and/or ion movement due to convection in the anterior chamber. Resolving this question requires further investigation.

With the assumption that Mn^{2+} ion follows the electric current (composed of all ions available in the electric current pathway), the distribution of the probe ion during iontophoresis can be used to assess the current paths during iontophoresis. Although the present electrode design did not have a seal surrounding the electrode–eye contact surface (Fig. 1A), only a small amount of Mn^{2+} was distributed to the surface of the eye outside the area underneath the electrode (total amount of Mn^{2+} outside on the eye surface is estimated to be less than 10% of the initial amount in the electrode device). Most ions were delivered into the eye during iontophoresis. The electric current pathways during iontophoresis were mainly from the electrode into the eye, perpendicular to the electrode–eye interface. There was some current distributed laterally along the sclera structure after penetration. Although the electric current passed through the globe between the donor electrode device and the return electrode, migration of the ion was slow and did not allow sufficient delivery of the ion (below the detection limit) to the back of the eye over the duration of the present experiments. The results in the present anodal iontophoresis study should also hold for cathodal iontophoresis, provided that the electric current distribution across the eye follows Ohm's law. However, different electrical polarities may induce different membrane and tissue structural changes. Future studies will examine this question when an anionic contrast agent becomes available.

Safety of Iontophoresis

Iontophoresis can enhance the penetration of a compound by altering the structure of a biological membrane.[6] If membrane alterations are reversible and do not cause any significant side effects, iontophoresis can be considered safe. The issue of safety related to ocular iontophoresis is beyond the scope of the present study as several recent studies have already discussed this topic.[9–12,22] Nevertheless, it deserves some attention. Both transscleral and transcorneal iontophoresis is relatively safe, provided the electric current density is low.[12,23] Although no histology was performed in the present study, the present transscleral iontophoresis parameters (total current, current density, and current duration) were chosen based on these previous studies. For example, Parkinson et al.[22] have shown that human subjects can tolerate (with no significant side effect) the electric current and current dose similar to those in the present study. Similar total current levels were also shown not to cause any observable side effects in the eye in other studies.[11,12,23] Whereas the transscleral iontophoresis parameters in the present study were justified, the parameters of transcorneal iontophoresis were chosen to be the same as those of transscleral iontophoresis to allow direct comparison between these two methods. As a result, the duration of the transcorneal iontophoresis (30 minutes) was longer than those typically used in previous studies ($\leq$10 minutes),[9,10,23,24] and such applications could lead to corneal damage. With the electrode design and iontophoresis protocol in the present study, both transscleral and transcorneal iontophoresis also caused minor silver burn at the sites of iontophoresis (electric current-driven silver ions precipitating at the eye surface). The silver burn disappeared within several days.

Pharmacokinetic Studies with MRI

The lack of understanding of the mechanisms of ocular drug delivery, pharmacokinetics, distribution, and elimination is partly due to the complicated anatomy of the eye.[25] It is also a result of the lack of data due to the invasive approaches taken to study drug distributions in the eye. These invasive approaches are expensive and inconvenient, severely perturb the eye during sampling, and require large numbers of animals in each study. For example, traditional pharmacokinetic studies involve killing animals at different time points after drug administration and assaying different sections of the eye for the drug. A noninvasive approach to the study of ocular pharmacokinetics and drug delivery not only can reduce the number of animals required in ocular drug delivery and pharmacokinetic research, but also allows the determination of the concentration profiles in the vitreous on a real-time basis without perturbation. Sampling of the eye by dissection in traditional pharmacokinetic studies may also result in redistribution of the compound of interest in the eye during assay. MRI can be used to determine the distribution and route of elimination of ions and compounds during and after ocular drug delivery such as iontophoresis, intravitreal injection, and periocular injection without these drawbacks. It is a promising noninvasive complementary technique to the traditional methods.

Although MRI has been used in ocular research previously,[14,26] the present study is the first to use MRI as a noninvasive method to retrieve real-time information on the pharmacokinetics and elimination of an ion in the eye. Although the present study has only demonstrated the use of a probe ion in ocular noninvasive pharmacokinetic studies, MRI can be used to monitor the pharmacokinetics and elimination of compounds labeled with a chelating moiety bound to magnetic ions such as diethylene triamine pentaacetic acid (DTPA). The MRI technique can also be used to monitor liposomal and micellar ocular drug delivery[27] when the liposomes and micelles are loaded or labeled with Mn or gadolinium (Gd) probes. However, quantitative MRI analyses at this stage are limited to the vitreous and aqueous humor. Additional calibration studies and further fine tuning of the technique are necessary before accurate measurements of the concentration of contrast agents in eye tissues can be obtained.

Acknowledgments

The authors thank David J. Miller for help in the electrode design and helpful discussion; Rajan P. Kochambilli for preparing the experiments; William I. Higuchi and Dennis L. Parker for suggestions; Paul S. Bernstein for helpful discussion and demonstrating the injection techniques; and Steven L. Hamilton for information on the field of ocular drug delivery.

References

1. Geroski DH, Edelhauser HF. Transscleral drug delivery for posterior segment disease. *Adv Drug Deliv Rev*. 2001;52:37–48.
2. Kasting GB. Theoretical models for iontophoretic delivery. *Adv Drug Deliv Rev*. 1992;9:177–199.
3. Li SK, Ghanem AH, Peck KD, Higuchi WI. Iontophoretic transport across a synthetic membrane and human epidermal membrane: a study of the effects of permeant charge. *J Pharm Sci*. 1997;86:680–689.
4. Pikal MJ. The role of electroosmotic flow in transdermal iontophoresis. *Adv Drug Deliv Rev*. 1992;9:201–237.
5. Peck KD, Srinivasan V, Li SK, Higuchi WI, Ghanem AH. A quantitative description of the effect of molecular size upon electroosmotic flux enhancement during iontophoresis for a synthetic membrane and human epidermal membrane. *J Pharm Sci*. 1996;85:781–788.
6. Li SK, Ghanem AH, Peck KD, Higuchi WI. Pore induction in human epidermal membrane during low to moderate voltage iontophoresis: a study using AC iontophoresis. *J Pharm Sci.* 1999;88:419–427.
7. Lachaud JP. Consideration on the use of corticoids by ionization in certain ocular diseases [in French]. *Bull Soc Ophtalmol Fr*. 1965;65:84–90.
8. Lam TT, Edward DP, Zhu XA, Tso MO. Transscleral iontophoresis of dexamethasone. *Arch Ophthalmol.* 1989;107:1368–1371.
9. Yoo SH, Dursun D, Dubovy S, et al. Iontophoresis for the treatment of paecilomyces keratitis. *Cornea*. 2002;21:131–132.
10. Behar-Cohen FF, Parel JM, Pouliquen Y, et al. Iontophoresis of dexamethasone in the treatment of endotoxin-induced-uveitis in rats. *Exp Eye Res*. 1997;65:533–545.
11. Behar-Cohen FF, El Aouni A, Gautier S, et al. Transscleral coulomb-controlled iontophoresis of methylprednisolone into the rabbit eye: influence of duration of treatment, current intensity and drug concentration on ocular tissue and fluid levels. *Exp Eye Res*. 2002;74:51–59.
12. Voigt M, Kralinger M, Kieselbach G, et al. Ocular aspirin distribution: a comparison of intravenous, topical, and coulomb-controlled iontophoresis administration. *Invest Ophthalmol Vis Sci*. 2002;43:3299–3306.
13. Kreft BP, Baba Y, Tanimoto A, Finn JP, Stark DD. Orally administered manganese chloride: enhanced detection of hepatic tumors in rats. *Radiology*. 1993;186:543–548.
14. Watanabe T, Michaelis T, Frahm J. Mapping of retinal projections in the living rat using high-resolution 3D gradient-echo MRI with Mn^{2+}-induced contrast. *Magn Reson Med*. 2001;46:424–429.
15. Stark DD, Bradley WG. *Magnetic Resonance Imaging.* 2nd ed. St. Louis: Mosby Year Book; 1992:chap 14.
16. Bard AJ, Faulkner LR. *Electrochemical Methods: Fundamentals and Applications.* New York: John Wiley & Sons; 1980.
17. Crank J. *The Mathematics of Diffusion.* 2nd ed. New York: Oxford University Press; 1975.
18. Pautler RG, Mongeau R, Jacobs RE. In vivo trans-synaptic tract tracing from the murine striatum and amygdala utilizing manganese enhanced MRI (MEMRI). *Magn Reson Med*. 2003;50:33–39.

19. Schoenwald RD. In: Zimmerman TJ, Kooner KS, Sharir M, Fechtner RD, eds. *Textbook of Ocular Pharmacology.* Philadelphia: Lippincott-Raven; 1997:chap 9.
20. Horibe Y, Hosoya K, Kim KJ, Ogiso T, Lee VH. Polar solute transport across the pigmented rabbit conjunctiva: size dependence and the influence of 8-bromo cyclic adenosine monophosphate. *Pharm Res*. 1997;14:1246–1251.
21. Hamalainen KM, Kananen K, Auriola S, Kontturi K, Urtti A. Characterization of paracellular and aqueous penetration routes in cornea, conjunctiva, and sclera. *Invest Ophthalmol Vis Sci*. 1997; 38:627–634.
22. Parkinson TM, Ferguson E, Febbraro S, Bakhtyari A, King M, Mundasad M. Tolerance of ocular iontophoresis in healthy volunteers. *J Ocul Pharmacol Ther*. 2003;19:145–151.
23. Hughes L, Maurice DM. A fresh look at iontophoresis. *Arch Ophthalmol*. 1984;102:1825–1829.
24. Grossman RE, Chu DF, Lee DA. Regional ocular gentamicin levels after transcorneal and transscleral iontophoresis. *Invest Ophthalmol Vis Sci*. 1990;31:909–916.
25. Worakul N, Robinson JR. Ocular pharmacokinetics/pharmacodynamics. *Eur J Pharm Biopharm*. 1997;44:71–83.
26. Alikacem N, Yoshizawa T, Nelson KD, Wilson CA. Quantitative MR imaging study of intravitreal sustained release of VEGF in rabbits. *Invest Ophthalmol Vis Sci*. 2000;41:1561–1569.
27. Barza M, Stuart M, Szoka F Jr. Effect of size and lipid composition on the pharmacokinetics of intravitreal liposomes. *Invest Ophthalmol Vis Sci*. 1987;28:893–900.